Dual-SLAM:
A framework for robust single camera navigation

Huajian Huang, Wen-Yan Lin*, Siying Liu, Dong Zhang, Sai-Kit Yeung

Abstract— SLAM (Simultaneous Localization And Mapping) seeks to provide a moving agent with real-time self-localization. To achieve real-time speed, SLAM incrementally propagates position estimates. This makes SLAM fast but also makes it vulnerable to local pose estimation failures. As local pose estimation is ill-conditioned, local pose estimation failures happen regularly, making the overall SLAM system brittle. This paper attempts to correct this problem. We note that while local pose estimation is ill-conditioned, pose estimation over longer sequences is well-conditioned. Thus, local pose estimation errors eventually manifest themselves as mapping inconsistencies. When this occurs, we save the current map and activate two new SLAM threads. One processes incoming frames to create a new map and the other, recovery thread, backtracks to link new and old maps together. This creates a Dual-SLAM framework that maintains real-time performance while being robust to local pose estimation failures. Evaluation on benchmark datasets shows Dual-SLAM can reduce failures by a dramatic 88%.

I. INTRODUCTION

Simultaneous Localization And Mapping or SLAM, seeks to provide a moving agent with a real-time reconstruction of its surroundings. SLAM plays a key role in tasks such as path planning, collision avoidance and self-localization. This paper focuses on monocular SLAM, which computes the three-dimensional map from a single moving camera. While this is the most brittle of the SLAM formulations, it is also the most general. This means lessons learned from monocular SLAM can be readily applied to many other SLAM formulations.

Monocular SLAM works by propagating pose estimates through a sequence of frames. The propagation makes SLAM fast. However, it also makes SLAM brittle, as a single erroneous pose can create inconsistencies that destroy the map. This problem is exacerbated by the fact that pose estimation on short sequences is ill-conditioned. Thus, occasional pose estimation errors are almost unavoidable.

Although pose estimation over short sequences (narrow baselines) is ill-conditioned, pose estimation over longer sequences (wide baselines) is well-conditioned. This causes SLAM failures to exhibit a distinctive pattern. Extreme local errors seldom propagate indefinitely. Instead, the well-conditioned nature of wide baseline pose estimation means

Huajian Huang and Sai-Kit Yeung are with the Department of Computer Science and Engineering, Hong Kong University of Science and Technology.

Wen-Yan Lin*, corresponding author, is with the School of information systems, Singapore Management University.

Siying Liu is with Institute for Infocomm Research, Singapore.

Dong Zhang is with the School of Electronics and Information Technology, Sun Yat-sen University.

Fig. 1: Sequence 09 of KITTI [1]. Left: ORB-SLAM's [2] map. Right: Dual-SLAM's map. Regions where recovery is needed are indicated in red (best viewed in color).

that if a map becomes erroneous, inconsistencies with incoming frames eventually emerge. Hence, SLAM seldom (if ever) creates a randomly incorrect map; instead, it tends to break when errors occur.

Given this failure pattern, local pose estimation errors are easy to rectify. We demonstrate this with a Dual-SLAM framework. Dual-SLAM utilizes the same incremental pose estimation as traditional SLAM. When significant mapping inconsistencies manifest themselves, we save the current map and initialize two new SLAMs. One SLAM starts a new map that incorporates the incoming key-frames. The other, called recovery SLAM, propagates the new map in the opposite direction to join with the old map, thus by-passing the corrupted section.

This framework avoids the high computational cost needed to prevent any possible pose estimation failure [3], [4] but provides stability, as the overall Dual-SLAM framework only fails if both the main and recovery SLAM threads fail simultaneously. This maintains real-time performance while removing much of the frustrating brittleness plaguing monocular SLAM. Tests on standard benchmarks show that Dual-SLAM can reduce failures by a dramatic 88%. An example is shown in Figure 1.

A. Related Works

Monocular SLAM's brittleness is widely acknowledged by the community. To date, the primary solution is to avoid

the problem by adding more sensing modalities. Examples include depth sensors [5], inertial measurement units [6]–[8] and stereo cameras [9], [10]. Such solutions greatly improve SLAM's robustness as the overall system only fails if all modalities fail simultaneously. The drawback of this approach is it often results in very complicated systems. This is because all modalities must be calibrated with respect to each other. Further, calibration drifts over time, thus requiring constant re-estimation [11]. Despite its limitations, multi-modality SLAM is (in our opinion), more practical than monocular SLAM. However, the question remains. Can monocular SLAM be fundamentally stabilized?

Before attempting to answer this question, a distinction must be made between two different SLAM problems. The first is a SLAM where the camera is restricted to moving within a small area. Monocular SLAM is already stable on such problems. Since the scene is small, the three dimensional map can be assumed to have been recovered accurately (there is no time to fail). Once this is achieved, the SLAM needs never fail as it can use a loop-closure detection module to re-localize itself with respect to the map. This philosophy is exploited with startling success in PTAM [5].

The second SLAM problem involves an agent roaming a large region and rarely revisiting the same place. Such problems are often termed video odometry. In this case, SLAM's mapping needs to remain stable over extended periods of time, without relying on prior maps for guidance. This is a much more difficult problem, that we seek to address with the Dual-SLAM framework.

While Dual-SLAM estimates camera pose from tracked feature points, there also exists works that employ direct pose estimation. Notable examples include LSD-SLAM [12] and LDSO [13] which directly use image color information to supplement feature tracking. Direct pose estimation allows SLAM algorithms to make reasonable pose estimates on even difficult scenes. Their drawback is that it is hard to run bundle-adjustment on such frameworks. This lowers the overall quality of pose estimates. We show that Dual-SLAM makes traditional SLAM nearly as stable as direct pose estimation while maintaining excellent accuracy. More excitingly, merging Dual-SLAM with direct matching offers the possibility of extreme accuracy and stability.

Finally, we use ORB-SLAM [9] as the base SLAM for our Dual-SlAM framework. ORB-SLAM is itself an adaptation of classical Structure-from-Motion to real-time execution on video frames. Thus, ORB-SLAM (and by extension Dual-SlAM) relies on many Structure-from-Motion modules like RANSAC [14], feature correspondence [3], [4], [15], [16], epipolar geometry [17]–[19], loop-closure detection [20] and global map building [21], [22].

II. OUR APPROACH

Our approach is based on the following hypothesis regarding SLAM errors.

To provide real-time self-localization, SLAM incrementally propagates narrow baseline pose estimates. However, as shown in Figure 2 narrow baseline pose estimation is
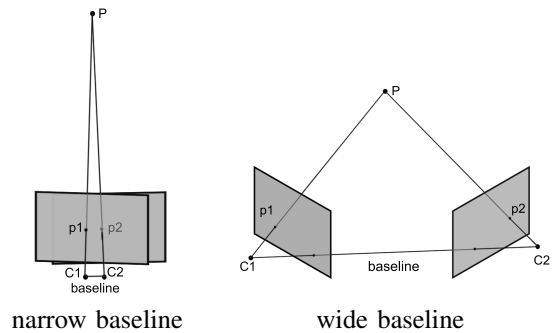

narrow baseline   wide baseline

Fig. 2: Pose estimation is based on triangulation. Narrow baseline triangulation is ill-conditioned because it is based on the intersection of two near-parallel lines. In contrast, wide baseline triangulation is much better conditioned. This creates a unique SLAM failure pattern which is easy to rectify.

innately ill-conditioned [23]; thus, small errors in input (feature correspondence) can result in large errors in the answer (pose estimates). As such, extreme errors in local pose estimation are almost inevitable.

These local pose errors create a corresponding, erroneous map that may not be immediately recognizable as being incorrect. However, as the baseline gets wider and triangulation better conditioned, it becomes harder for newly tracked points to be consistently fused with the erroneous map. This causes the SLAM sequence to break.

If the above hypothesis is true, many breakages that appear like tracking failures may actually be due to stochastic errors in pose estimation. This motivates us to introduce the Dual-SLAM framework for enhanced SLAM robustness.

At its core, Dual-SLAM is a normal SLAM with a modified handling of tracking failure. When traditional SLAM encounters tracking failures, it typically considers the scene too difficult and breaks. In contrast, Dual-SLAM assumes that tracking failures are due to stochastic pose estimation errors. Thus, instead of accepting the failure, Dual-SLAM saves the old map and restarts a new SLAM to create a new map from incoming frames. At the same time, Dual-SLAM runs a recovery SLAM backward in time, to bridge the old and new maps. A schematic overview of the system is presented in Figure 3.

A. Statistical Analysis of Dual-SLAM

From a statistical viewpoint, Dual-SLAM increases system reliability through redundancy. We model a SLAM's pose estimator's failure as a stochastic process. Let the probability of a SLAM system failing over a unit sequence length be p_0, and let the probability of recovery thread failure be p_r. As the recovery thread is run independently of the original SLAM map, the probability of Dual-SLAM failure with one recovery thread is, therefore, $Pr(Failure) = p_0 \times p_r$. Given n independent recovery threads, the overall failure probability is given by:

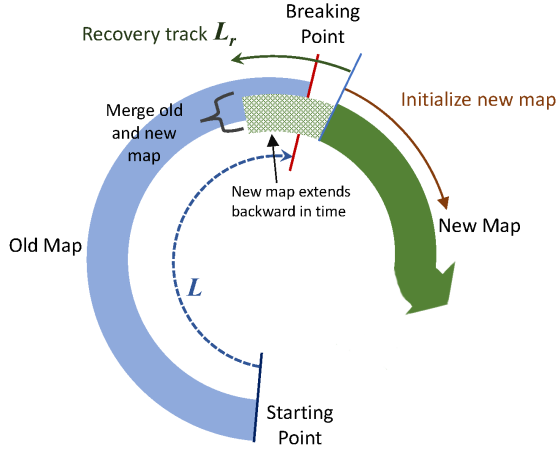$$Pr(Failure) = p_0 \times (p_r)^n \qquad (1)$$

Fig. 3: Dual-SLAM handles sequence breakages by saving the existing map and starting two SLAMs. One creates a new map that propagates forward in time. The other SLAM propagates map backward in time to link the new map with the old one. We show that empirically and statistically, this framework provides outstanding stability.

Fig. 4: The buffer queue stores frames over which the recovery SLAM propagates. The size of the window $K = k + k_r$ is adaptive.

If both the base system and the recovery thread use the same pose estimator, we have $p_r = p_0$, since the pose estimation algorithm is considered to behave the same way in both forward and backward directions. Note that since the recovery thread can utilize information from earlier frames stored in the memory, it is intrinsically faster. This time advantage can be exploited by using slower but more reliable methods, such as SIFT [16] features, in place of generic ORB features. Thus, p_r is generally lower than p_0.

Due to the multiplicative nature of Eq. (1), the failure probability can drop dramatically. Consider a case where $p_0 = 0.1$, $n = 1$ and $p_r = 0.1$. A standard SLAM would have a failure probability of $Pr(Failure) = 0.1$. In contrast, Dual-SLAM with one recovery thread will have failure probability reduced to 0.01. This means Dual-SLAM can survive over dramatically longer sequences than its base SLAM. While Dual-SLAM eliminates much of the random failures plaguing traditional SLAM, it does not solve all problems. In particular, it cannot solve intrinsically difficult cases, such as scenes with low texture. In such cases, p_0 and p_r are close to 1 and irrespective of the number of recovery threads, the probability of failure is still very high, i.e. $Pr(Failure) \approx 1$.

III. SYSTEM IMPLEMENTATION

Our base system uses ORB-SLAM [2], an excellent implementation of feature-based monocular SLAM. ORB-SLAM has three primary threads. The first is a tracking thread that incrementally maps an agent's location; the second is a local-mapping thread that processes new key-frames to incrementally expand the map; the last is a loop-closure thread that reduces drift if an agent revisits a previously visited location. ORB-SLAM's tracking thread predicts cam-
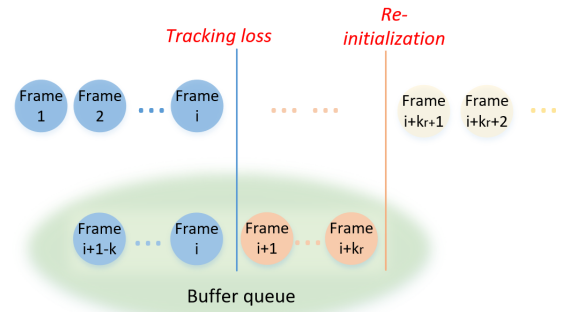
era pose using feature matches and the previous camera pose estimate. Poses are refined by a background bundle-adjustment thread and incorporated into a 3D map. When pose predictions are incorrect, an error occurs in the 3D map; as the camera moves onward, incoming features are increasingly inconsistent with the now erroneous 3D map, leading to an apparent "tracking failure".

Dual-SLAM primarily modifies the handling of "tracking failures". Upon encountering a "tracking failure", another tracking thread is immediately spawned to handle incoming frames and initialize a new map from them. This new map is temporarily disconnected from the old. To reconnect them, a recovery SLAM is started from the new map's first frame and propagates backward in time. This extends the new map till it obtains sufficient sparse co-visibility 3D key-points with the old map for a merger.

Details of the modification are provided below.

A. Buffering

To make recovery as efficient as possible, it is necessary for Dual-SLAM to maintain a buffer of ORB features. During Dual-SLAM's normal operation, the ORB features of the most recent k frames, are stored in a constantly updated buffer queue. The buffer must be large enough to ensure an overlap with un-corrupted portions of the map; however, it cannot be so large that storage cost becomes prohibitive. Empirically, we find setting k to the number of frames in 10 seconds of video duration works well.

Under normal operating conditions, the buffer acts as a queue, with new frames being added and an equal number of the oldest frames being removed. When tracking fails, frames are no longer removed from the buffer. However, new frames are added to the buffer until the new map is re-initialized successfully. If re-initialization occurs after k_r frames, the overall buffer length is extended to $K = k + k_r$, as shown in Figure 4. Since recovery thread's SLAM is run over this buffer, the amount of time needed to recover maps is proportional to K. The more delayed the re-initialization is, the more time is needed for recovery.

Algorithm 1 Recovery thread

Require:
    buffer: $K, F_{i+k_r} \rightarrow F_{i+1-k}$;

1:
2:   /∗ Recovery thread 1/∗
3:   **for** frame $F_j \in K$ **do**
4:      pose: p_j from motion model;
5:      tracked points: t_j conforming to motion p_j;
6:      **if** number of tracked points less than threshold **then**
7:        break; /∗ Recovery thread 1 unsuccessful/∗
8:      **end if**
9:   **end for**
10: Parallel running of bundle-adjustment point cloud reconstruction using ORB-features and p_j poses.
11: **if** Recovery thread 1 successful **then**
12:     **return** 3D-points
13: **end if**
14:
15: /∗ Recovery thread 2/∗
16: **for** frame $F_i \in K$ **do**
17:     $S_j = SIFT_{match}(F_j, F_{j-1})$
18:     pose: $p_j = PnP(S_j)$
19: **end for**
20: Parallel running of bundle-adjustment point cloud reconstruction using ORB-features and p_j poses.
21: **if** Recovery thread 2 successful **then**
22:     **return** 3D-points
23: **else**
24:     **return** failure
25: **end if**

B. Recovery thread

Two different recovery threads are run sequentially. The first recovery thread is similar to a basic ORB-SLAM. If the first recovery thread fails, i.e. ORB-SLAM is unable to propagate pose throughout the buffer, the second recovery SLAM is activated. This SLAM uses SIFT [16] features and a PnP [24] based pose estimation. The procedure is summarized in algorithm 1.

After the recovery thread processes all buffer frames, the new map will have 3D points that overlap with the old map. We use these common points to fuse the maps.

C. Map Fusion

Old and new maps are related by a 3D similarity transformation, which if estimated, will enable the fusion of the two maps. As the recovery thread has extended the new map backward over the buffer, it now has 3D key-points whose locations overlap with those of the old map. We use these 3D key-points to estimate the required similarity transformation.

Each key-point has a corresponding key-frame ID. This means that for each key-point in the new map, its candidate key-point matches in the old map can be restricted to only those with similar key-frame IDs. This limits the search to a small portion of the map.
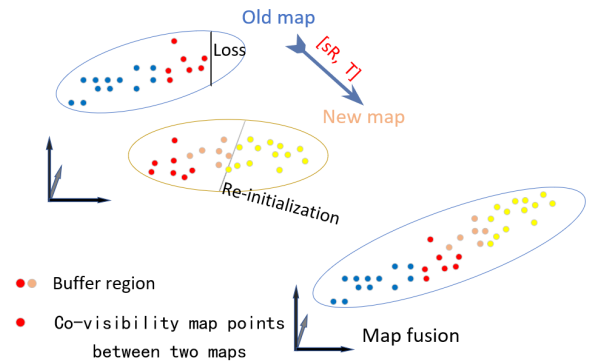

Fig. 5: Fusing old and new maps with the buffer region.

The final matching is decided on the basis of ORB features descriptors. The result is a set of 3D-to-3D match hypotheses. If $\mathbf{X}_j, \mathbf{X}'_j$ are a pair of matched 3D points from the old and new maps respectively, they will be related by the expression:

$$\mathbf{X}'_j = s\mathbf{R}\mathbf{X}_j + \mathbf{T}, \tag{2}$$

where $\mathbf{R}$ is a 3×3 rotation matrix, $\mathbf{T}$ is a 3×1 translation matrix, and s is a scaling factor. The similarity transformation parameters $s, \mathbf{R}, \mathbf{T}$ can be estimated by applying RANSAC with Horn's [25] algorithm. This similarity transform allows the merger of the maps, as shown in Figure 5. After the merger, SLAM can resume normal operation.

D. Enhanced version: Dual-SLAM$^+$

As mentioned earlier in Sec. III-A, rapid initialization is important to Dual-SLAM's performance. To achieve this, we modify ORB-SLAM's initialization with an advanced feature matching based on the GMS [26] algorithm. We term this enhanced version Dual-SLAM$^+$.

This modification prevents the often unacceptable lag that occurs with basic Dual-SLAM, greatly improving overall performance as demonstrated in Figure 6.

IV. EVALUATION

We evaluate the proposed algorithm on KITTI [1] visual odometry and TUM [27] monocular datasets. These afford a wide variety of scenarios including outdoor, indoor and on-road scenes. Experiments are performed on an Intel Core i7-6700K laptop. As SLAM is non-deterministic, in all experiments, we perform 10 trials on each sequence.

A. Comparisons

We benchmark Dual-SLAM against both classic baseline SLAM systems and new state-of-the-art SLAM algorithms. ORB-SLAM [2], a feature-based monocular SLAM system is used as the baseline. This is a classic SLAM algorithm that requires no further introduction. LDSO [13] represents the current state-of-the-art. It is a sophisticated SLAM framework that fuses traditional feature correspondence with direct image differences and pose-graph optimization. We find LDSO's performance is significantly better than its predecessors, LSD-SLAM [12] and DSO [28].
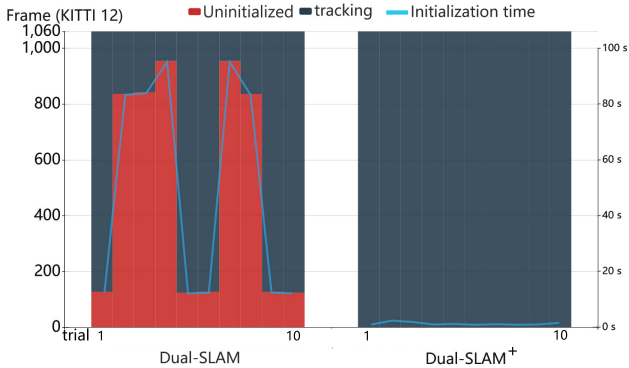
Fig. 6: Comparison of initialization performance on the KITTI 12. This sequence contains 1060 frames. Horizontal axis: 10 different trials. Left vertical axis: initialization time in sequence frames numbers. Right vertical axis: initialization time (s). Out of 10 trials, on average, Dual-SLAM takes 50.51s to initialize, while Dual-SLAM$^+$ takes 0.5s.
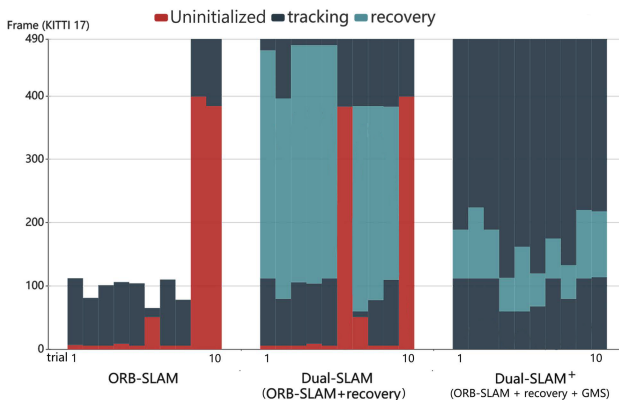

Fig. 7: Comparing SLAM algorithms on KITTI, sequence 17. Horizontal axis: Trial number. Vertical axis: Frame index. ORB-SLAM fails early in the sequence, leaving most of its profile white. Dual-SLAM can recover from the failure, providing a complete map. However, the recovery is very slow. Finally, Dual-SLAM$^+$demonstrates rapid recovery, making the overall navigation system more viable.

In evaluations, we use ORB-SLAM at default parameters but make minor modifications to LDSO. This is because LDSO at default parameters, often terminates prematurely on easy KITTI sequences. We find that this is due to the sensitivity of LDSO's loop-detection module. Thus, to make the comparisons more meaningful, we modify LDSO's loop-detection sensitivity for KITTI sequences.

B. KITTI Dataset

The KITTI [1] visual odometry dataset is captured from a vehicle. It includes scenes from urban and rural areas, as well as highways. The high speed of the data acquisition vehicle coupled with occasional rapid rotations, make KITTI especially challenging.

TABLE I: Results on the KITTI [1]. Each sequence is run 10 times for a total of 110 trials. The median RMSEs of the keyframes trajectory is reported. Dual-SLAM$^+$ maintains ORB-SLAM's accuracy but is more stable. These results are comparable with state-of-art, LDSO.

Sequence	ORB-SLAM RMSE(m)		Dual-SLAM RMSE(m)		Dual-SLAM$^+$ RMSE(m)		LDSO RMSE(m)
KITTI 00	8.18	⌒	7.48		**7.30**		9.30
KITTI 01	⊗	⊗	⊗	⊗	⊗	⊗	**10.31**
KITTI 02	24.11	⌒	24.74		**23.35**		25.73
KITTI 03	**1.18**		1.29		1.25		2.14
KITTI 04	1.65		1.39		1.20		**0.79**
KITTI 05	8.23		8.23		6.26		**5.43**
KITTI 06	15.84		17.86		13.29		**12.57**
KITTI 07	2.43		2.50		2.59		**1.54**
KITTI 08	51.34	⌒	50.23		**49.99**		115.90
KITTI 09	50.69	⌒	13.72		**6.97**		70.59
KITTI 10	7.68		7.68		**6.92**		14.79
Failure trial	28		10		6		0

⊗ : the system cannot process the sequence map at all
⌒ : the system has possibilities of tracking failure on this sequence

The KITTI dataset contains 22 sequences, of which 11 sequences (00-10) possess ground truth trajectories. Standard ORB-SLAM fails to construct an intact map on 5 sequences (KITTI 00, 01, 02, 08, and 09). Dual-SLAM reduces the failures to just one sequence, KITTI 01. The break-down of failures by individual sequences is presented in Tab. I. Observe that Dual-SLAM$^+$'s improvements are so large that it makes the older (and simpler) ORB-SLAM framework competitive with state-of-the-art LDSO SLAM. This is most evident on sequences 08, 09 and 10. A profiling of the Dual-SLAM algorithm is provided in Figure 7, with visual comparison on selected sequences presented in Figure 8.

C. TUM-Mono Dataset

TUM [27] monocular visual odometry dataset contains 50 sequences, recorded in both outdoor and indoor environments. Ground-truth camera trajectories are not available. However, as the agent moves in a loop, its start and end points are identical. Hence, accuracy can be measured through end-point error. Results are tabulated in Figure 9.

Figure 9 shows that ORB-SLAM's performance exhibits a distinctive dichotomy, with the system either failing completely or providing highly accurate maps. This supports our hypothesis that many of ORB-SLAM's errors are caused by stochastic pose estimation errors, which destroy an otherwise, very accurate map.

Dual-SLAM eliminates most of these errors. Thus, out of 500 trials, ORB-SLAM failed 126 times, while Dual-SLAM and Dual-SLAM$^+$ only failed 14 and 12 times respectively. The resultant Dual-SLAM system is arguably even better than the state-of-art LDSO [13].

Figure 10 shows a qualitative comparison on sequence 41 of TUM-Mono dataset. This is a challenging scene, where the agent navigates across two floors of an indoor environment.
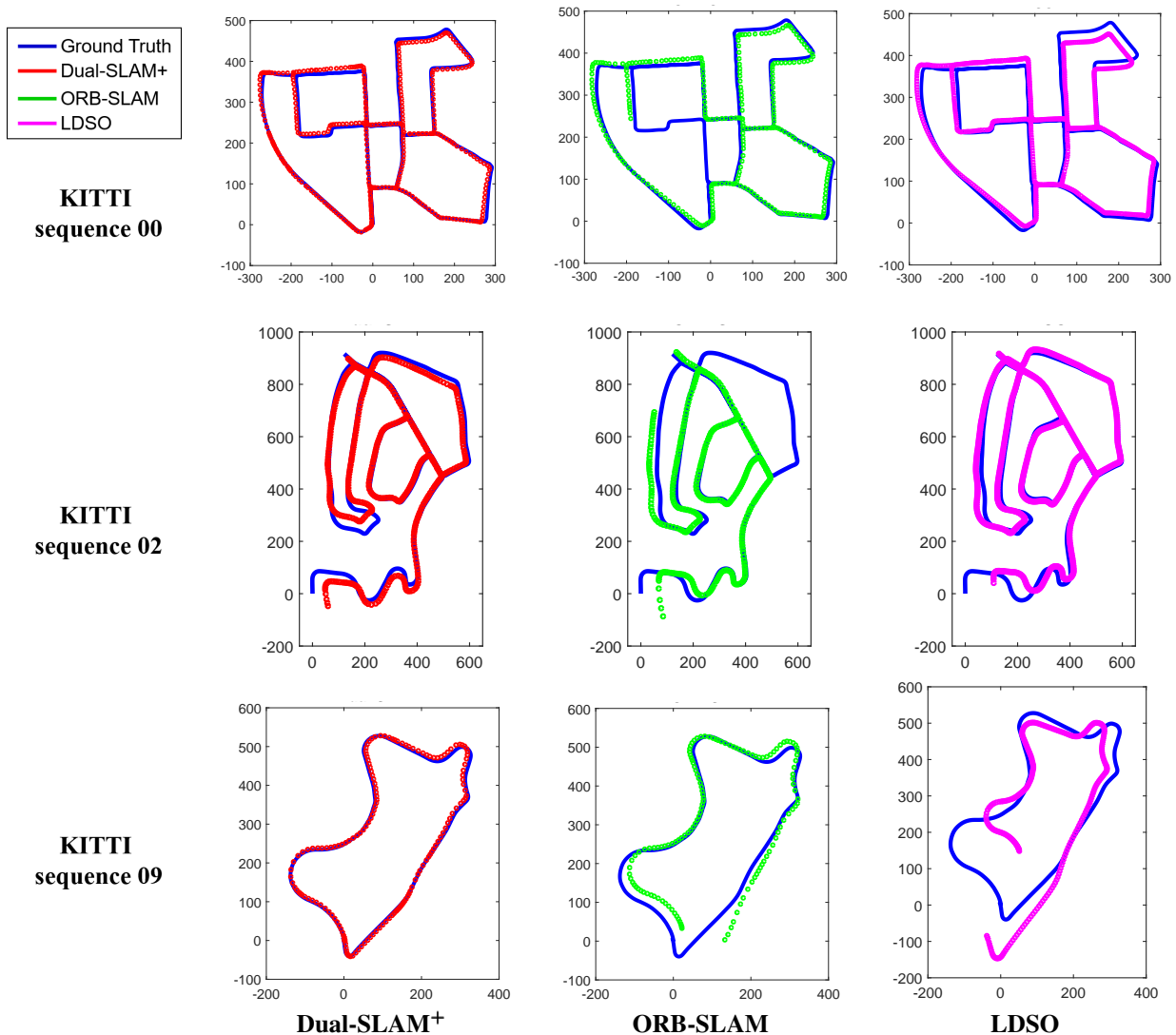
Fig. 8: Overlay of SLAM and ground-truth trajectories on KITTI sequences. Ground-truth is in blue. Ideally, the SLAM trajectory would completely cover the ground-truth, making it no longer visible. In cases where the SLAM breaks, large sections of ground-truth become visible. Observe that Dual-SLAM greatly improves ORB-SLAM's results, making it competitive with LDSO.

We observe that DUAL-SLAM is able to rescue breakages and perform accurate map fusion upon recovery. The result is a reconstruction of a much larger floor area.

V. ANALYSIS

A. Failure Rates

The evaluation section suggests that Dual-SLAM is much stabler than basic ORB-SLAM. Table II quantifies this, showing Dual-SLAM reduces failure rates by 84%-88%. This is a remarkable result for a relatively simple modification.

B. Ablation Study

Table III provides a break down of performance statistics based on the initialization (Dual-SLAM vs Dual-SLAM$^+$) and the number of recovery threads deployed. Dual-SLAM and Dual-SLAM$^+$ deployed recovery threads 153 and 156

TABLE II: Comparing failure rates of the base ORB-SLAM with our improved Dual-SLAM. Note that Dual-SLAM reduces the number of failures sharply.

	Failure rate = # failure / # trials		
	ORB-SLAM	Dual-SLAM	Dual-SLAM$^+$
KITTI [1]	28/110	10/110	6/110
TUM-Mono [27]	126/500	14/500	12/500
Total	154/610	24/610	18/610
Failure Reduction	N.A.	1-24/154 =0.84	1-18/154 = 0.88

times respectively. Successful recovery occur in 84.3% and 88.5% of the cases. Of these, in 95.3% and 95.7% of the cases, recovery was successful at the first attempt.

The high success of the first recovery thread has practical and theoretical implications. At a practical level, this phenomenon makes recovery much faster, enhancing Dual-
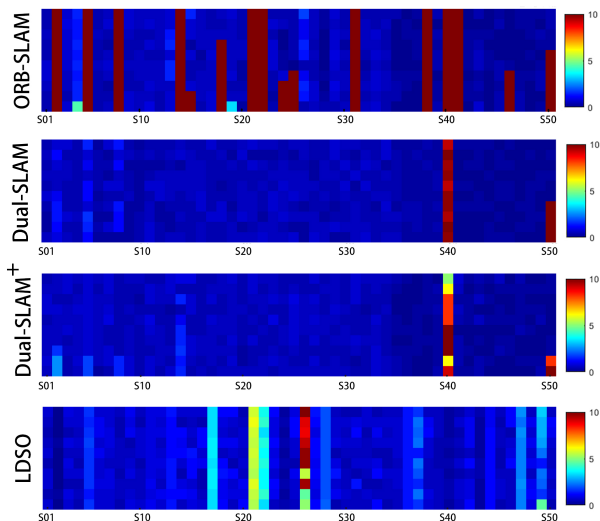
Fig. 9: Evaluation on TUM-Mono [27]. Horizontal axis: S01-S50 represents sequence names. Vertical axis: Results from 10 trials. Colors represent the end-point error in meters. Observe that traditional ORB-SLAM [2] alternates between high accuracy and total failure. Dual-SLAM eliminates 90.47% of the failures while maintaining its high accuracy.

TABLE III: Ablation study of performance on KITTI [1] and TUM-Mono [27] datasets. For both datasets, we run each sequence for 10 trials and deploy a maximum of two recovery threads in case of breakage. We tabulate the statistics of the number of times recovery is needed, the number of successful recoveries, the number of recovery threads used in the successful cases and the average time needed for recovery.

		Dataset		Average
		KITTI	TUM-Mono	Recovery Time
Dual-SLAM	Total Trials	110	500	16.30s
	Needs Recovery	28	125	
	Failure	10	14	
	Success	18	111	
	With 1 thread	17	106	
	With 2 threads	1	5	
Dual-SLAM+	Total Trials	110	500	9.37s
	Needs Recovery	30	126	
	Failure	6	12	
	Success	24	114	
	With 1 thread	22	110	
	With 2 threads	2	4	

SLAM's viability as a navigational technique. At a theoretical level, it validates Eq. (1) which predicts that a small amount of redundancy is sufficient to significantly reduce the likelihood of failure.

C. Relation to RANSAC

RANSAC is another algorithm that relies on stochastic pose prediction. In RANSAC, a small number of putative correspondences are used to estimate the pose between two frames. This process is iterated N times and the pose that is in agreement with the largest number of correspondences, is assumed to be the correct pose estimate.

Despite the superficial similarity between RANSAC and Dual-SLAM, more RANSAC iterations cannot solve the ill-conditioning of narrow baseline pose estimation as ill-conditioning implies the global minimum of a RANSAC cost may correspond to a highly incorrect pose estimate. Dual-SLAM addresses this problem by considering pose solutions over much wider baselines.

D. Framework Limitations

Dual-SLAM has two primary weaknesses. The first is its assumption that mapping errors always lead to breakages. As explained earlier, the well-conditioned nature of wide-baseline pose estimation makes this a good assumption. However, it is occasionally violated. When this occurs, the resultant maps often exhibit large drift errors. Note that in these cases the problems are not caused by the introduction of new errors but the result of a failure to correct existing errors. Examples of such failures are present in sequence 01 of KITTI and sequence 50 of TUM-Mono.

Dual-SLAM's other major weakness is its vulnerability to low textured scenes. This causes problems for all feature-based SLAM systems and Dual-SLAM is no exception. An example of this case occurs in sequence 40 of TUM-Mono.

E. Relation to LDSO and Future Work

Results in Table I and Figure 9 show that overall, Dual-SLAM's performance is comparable to LDSO. However, closer inspection reveals that the two techniques are very different, with each one favoring a different scene type. For general scenes, Dual-SLAM is typically more stable and accurate. However, LDSO has an advantage on scenes with extremely low textures or high motion blur.

These strengths and weaknesses are the result of different design philosophies. Dual-SLAM assumes tracking errors are the result of pose estimation failures, which it attempts to correct through re-estimation. In contrast, LDSO assumes tracking failures are the result of insufficient features, which it attempts to rectify trough dense matching.

We believe that neither the Dual-SLAM or LDSO approach is fully correct and that the ideal SLAM would be one that fuses both of these design philosophies. This offers the exciting potential for further performance improvements.

VI. CONCLUSION

This paper hypothesizes that the source of monocular SLAM brittleness is stochastic errors incurred by narrow baseline pose estimations. We develop a Dual-SLAM framework to address this problem, creating a simple but general framework for enhanced SLAM performance.
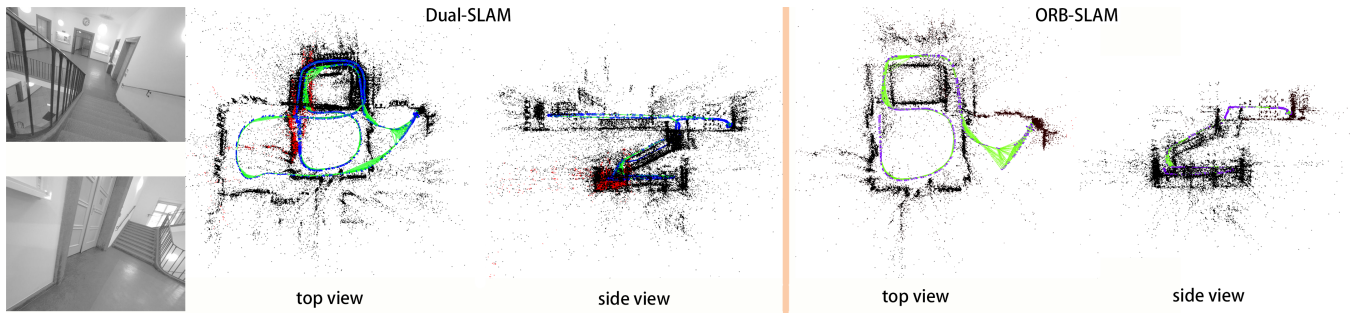
Fig. 10: Sequence 41 of TUM-Mono. Reconstructed 3D points are shown in black, key-frames in blue, linkages between adjacent frames in green and breakage locations in red. Dual-SLAM is stable on this very difficult sequence, allowing it to recover much more of the map than the original ORB-SLAM.

REFERENCES

[1] A. Geiger, P. Lenz, and R. Urtasun, "Are we ready for autonomous driving? the kitti vision benchmark suite," *IEEE Conference on Computer Vision and Pattern Recognition (CVPR)*, vol. 157, no. 10, pp. 3354–3361, 2012.

[2] R. Mur-Artal, J. M. M. Montiel, and J. D. Tardos, "Orb-slam: a versatile and accurate monocular slam system," *IEEE Transactions on Robotics*, vol. 31, no. 5, pp. 1147–1163, 2015.

[3] W.-Y. Lin, S. Liu, N. Jiang, M. N. Do, P. Tan, and J. Lu, "Repmatch: Robust feature matching and pose for reconstructing modern cities," in *European Conference on Computer Vision*. Springer, 2016, pp. 562–579.

[4] W.-Y. Lin, F. Wang, M.-M. Cheng, S.-K. Yeung, P. H. Torr, M. N. Do, and J. Lu, "Code: Coherence based decision boundaries for feature correspondence," *IEEE transactions on pattern analysis and machine intelligence*, vol. 40, no. 1, pp. 34–47, 2017.

[5] G. Klein and D. Murray, "Parallel tracking and mapping for small ar workspaces," in *Proceedings of the 2007 6th IEEE and ACM International Symposium on Mixed and Augmented Reality*. IEEE Computer Society, 2007, pp. 1–10.

[6] R. Li, J. Liu, L. Zhang, and Y. Hang, "Lidar/mems imu integrated navigation (slam) method for a small uav in indoor environments," in *2014 DGON Inertial Sensors and Systems (ISS)*. IEEE, 2014, pp. 1–15.

[7] M. W. Achtelik, S. Lynen, S. Weiss, L. Kneip, M. Chli, and R. Siegwart, "Visual-inertial slam for a small helicopter in large outdoor environments," in *2012 IEEE/RSJ International Conference on Intelligent Robots and Systems*. IEEE, 2012, pp. 2651–2652.

[8] A. Concha, G. Loianno, V. Kumar, and J. Civera, "Visual-inertial direct slam," in *2016 IEEE International Conference on Robotics and Automation (ICRA)*. IEEE, 2016, pp. 1331–1338.

[9] R. Mur-Artal and J. D. Tardos, "Orb-slam2: an open-source slam system for monocular, stereo and rgb-d cameras," *IEEE Transactions on Robotics*, vol. 33, no. 5, 5, Oct 2017.

[10] J. Engel, J. Stückler, and D. Cremers, "Large-scale direct slam with stereo cameras," in *2015 IEEE/RSJ International Conference on Intelligent Robots and Systems (IROS)*. IEEE, 2015, pp. 1935–1942.

[11] L. Von Stumberg, V. Usenko, and D. Cremers, "Direct sparse visual-inertial odometry using dynamic marginalization," in *2018 IEEE International Conference on Robotics and Automation (ICRA)*. IEEE, 2018, pp. 2510–2517.

[12] J. Engel, T. Schöps, and D. Cremers, "Lsd-slam: Large-scale direct monocular slam," in *European conference on computer vision*. Springer, 2014, pp. 834–849.

[13] X. Gao, R. Wang, N. Demmel, and D. Cremers, "Ldso: Direct sparse odometry with loop closure," in *2018 IEEE/RSJ International Conference on Intelligent Robots and Systems (IROS)*. IEEE, 2018, pp. 2198–2204.

[14] M. A. Fischler and R. C. Bolles, "Random sample consensus: a paradigm for model fitting with applications to image analysis and automated cartography," *Communications of the ACM*, vol. 24, no. 6, pp. 381–395, 1981.

[15] E. Rublee, V. Rabaud, K. Konolige, and G. Bradski, "Orb: An efficient alternative to sift or surf," *IEEE International Conference on Computer Vision*, vol. 58, no. 11, pp. 2564–2571, 2011.

[16] D. G. Lowe *et al.*, "Object recognition from local scale-invariant features." in *iccv*, vol. 99, no. 2, 1999, pp. 1150–1157.

[17] H. Li and R. Hartley, "Five-point motion estimation made easy," in *18th International Conference on Pattern Recognition (ICPR'06)*, vol. 1. IEEE, 2006, pp. 630–633.

[18] D. Nistér, "An efficient solution to the five-point relative pose problem," *IEEE transactions on pattern analysis and machine intelligence*, vol. 26, no. 6, pp. 0756–777, 2004.

[19] H. C. Longuet-Higgins, "A computer algorithm for reconstructing a scene from two projections," *Nature*, vol. 293, no. 5828, p. 133, 1981.

[20] D. Gálvez-López and J. D. Tardós, "Bags of binary words for fast place recognition in image sequences," *IEEE Transactions on Robotics*, vol. 28, no. 5, pp. 1188–1197, October 2012.

[21] E. Olson, J. Leonard, and S. Teller, "Fast iterative optimization of pose graphs with poor initial estimates," 2006, pp. 2262–2269.

[22] R. I. H. B. Triggs, P. F. McLauchlan and A. W. Fitzgibbon, "Bundle adjustment a modern synthesis," *International Workshop on Vision Algorithms: Theory and Practice*, vol. 1883, no. 1883, pp. 298–372, 1999.

[23] D. Knoblauch, M. Hess-Flores, M. A. Duchaineau, K. I. Joy, and F. Kuester, "Non-parametric sequential frame decimation for scene reconstruction in low-memory streaming environments," in *International Symposium on Visual Computing*. Springer, 2011, pp. 359–370.

[24] V. Lepetit, F. Moreno-Noguer, and P. Fua, "Epnp: An accurate o (n) solution to the pnp problem," *International journal of computer vision*, vol. 81, no. 2, p. 155, 2009.

[25] B. K. P. Horn, "Closed-form solution of absolute orientation using unit quaternions," *J. Opt. Soc. Amer. A*, vol. 4, no. 4, pp. 629–C642, 1987.

[26] J. Bian, W.-Y. Lin, Y. Matsushita, S.-K. Yeung, T.-D. Nguyen, and M.-M. Cheng, "Gms: grid-based motion statistics for fast, ultra-robust feature correspondence," in *Proceedings of the IEEE Conference on Computer Vision and Pattern Recognition*, 2017, pp. 4181–4190.

[27] J. Engel, V. Usenko, and D. Cremers, "A photometrically calibrated benchmark for monocular visual odometry," in *arXiv:1607.02555*, July 2016.

[28] J. Engel, V. Koltun, and D. Cremers, "Direct sparse odometry," *IEEE transactions on pattern analysis and machine intelligence*, vol. 40, no. 3, pp. 611–625, 2018.